Third Edition

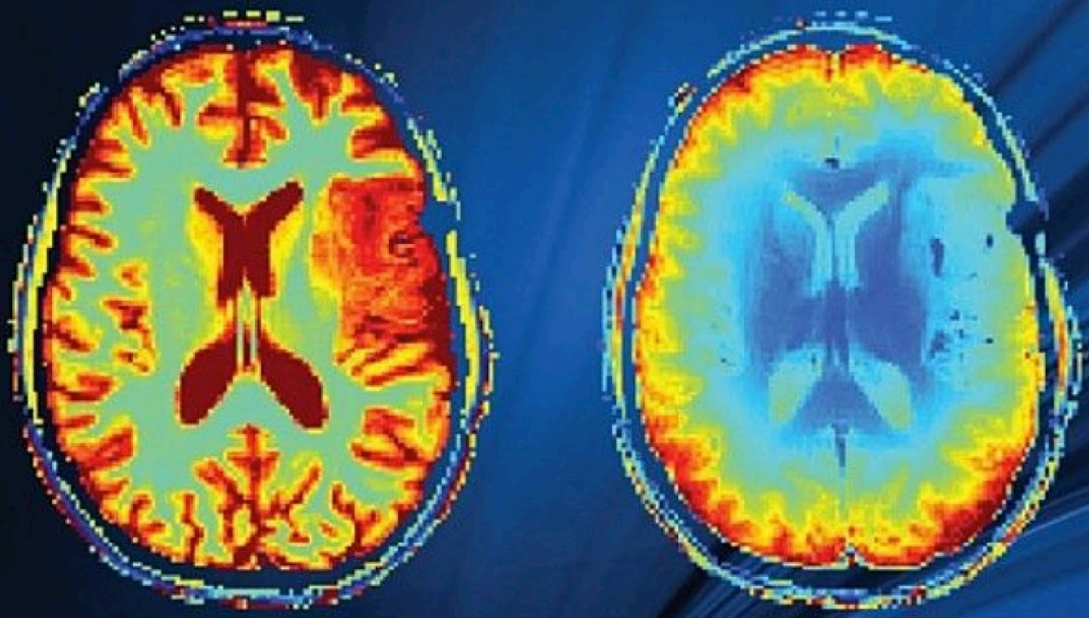

in vivo NMR Spectroscopy

Principles and Techniques

Robin A. de Graaf

WILEY

In Vivo NMR Spectroscopy

In Vivo NMR Spectroscopy

Principles and Techniques

Third Edition

Robin A. de Graaf

Department of Radiology and Biomedical Imaging
Department of Biomedical Engineering
Magnetic Resonance Research Center (MRRC)
Yale University
New Haven, CT, USA

WILEY

This edition first published 2019

Edition History
* 2007, Wiley, *In Vivo* NMR Spectroscopy: Principles and Techniques 2nd Edition
* 1998, Wiley, *In Vivo* NMR Spectroscopy: Principles and Techniques

Registered Offices
John Wiley & Sons, Inc., 111 River Street, Hoboken, NJ 07030, USA
John Wiley & Sons Ltd, The Atrium, Southern Gate, Chichester, West Sussex, PO19 8SQ, UK

Editorial Office
The Atrium, Southern Gate, Chichester, West Sussex, PO19 8SQ, UK

For details of our global editorial offices, customer services, and more information about Wiley products visit us at www.wiley.com.

Wiley also publishes its books in a variety of electronic formats and by print-on-demand. Some content that appears in standard print versions of this book may not be available in other formats.

Library of Congress Cataloging-in-Publication Data

Names: De Graaf, Robin A., author.
Title: *In vivo* NMR spectroscopy : principles and techniques / Robin A. de Graaf, Magnetic Resonance Research Center (MRRC), Yale University, Department of Radiology and Biomedical Imaging, Department of Biomedical Engineering, New Haven, CT, USA.
Description: Third edition. | Hoboken, NJ : Wiley, [2019] | Includes bibliographical references and index. |
Identifiers: LCCN 2018041668 (print) | LCCN 2018044006 (ebook) | ISBN 9781119382577 (Adobe PDF) | ISBN 9781119382515 (ePub) | ISBN 9781119382546 (hardback)
Subjects: LCSH: Nuclear magnetic resonance spectroscopy. | Magnetic resonance imaging. | BISAC: SCIENCE / Spectroscopy & Spectrum Analysis.
Classification: LCC QP519.9.N83 (ebook) | LCC QP519.9.N83 D4 2018 (print) | DDC 616.07/548–dc23
LC record available at https://lccn.loc.gov/2018041668

Cover design: Wiley
Cover image: Background ©ake1150sb; Other Images: Courtesy of the Author, Robin de Graaf

Set in 10/12pt Warnock by SPi Global, Pondicherry, India

10 9 8 7 6 5 4 3 2 1

In memory of Klaas Nicolay (1951–2017)

Contents

Preface

The main driving force to write a third edition was the inadequate description of several basic NMR phenomena in the earlier editions, as well as in the majority of NMR textbooks. The quantum picture of NMR provides the most general description that is applicable to all NMR experiments. As a result, the quantum description of NMR often takes center stage, but comes at the expense of forfeiting a physically intuitive picture. Inappropriate descriptions of NMR result when the quantum mechanics are incorrectly simplified to a classical picture. However, ever since the very first report on NMR in bulk matter by Felix Bloch, it is known that the NMR phenomenon for many compounds, like water, can be quantitatively described based on classical arguments without the need to invoke quantum mechanics. The current edition adopts this classical description for a very intuitive and straightforward description of NMR. While many aspects of *in vivo* NMR, including MR imaging, magnetization transfer, and diffusion can be successfully described, the classical description does prove inadequate in the presence of scalar coupling. At this point the classical description is replaced with a semiclassical correlated vector model that naturally leads to the quantum-mechanical product operator formalism.

The third edition also takes the opportunity to correct misconceptions about the nature of radiofrequency (RF) pulses and coils, and provides an updated review of novel methods, including hyperpolarized MR, deuterium metabolic imaging (DMI), MR fingerprinting, advanced magnetic field shimming, and chemical exchange saturation transfer (CEST) methods. However, it should be stressed that this book does not set out to present complete, detailed, and in-depth reviews of *in vivo* MRS methods.

The main objective of the book has always been to provide an educational explanation and overview of *in vivo* NMR, without losing the practical aspects appreciated by experimental NMR spectroscopists. This objective has been enhanced in this edition by relegating a significant number of mathematical equations to the exercises in favor of more intuitive, descriptive explanations and graphical depictions of NMR phenomena. The exercises are designed to review, but often also to extend the presented NMR principles and techniques, including a more in-depth exploration of quantitative MR equations. The textual description of RF pulses has been reduced and supplemented with PulseWizard, a Matlab-based RF pulse generation and simulation graphical user interface available for download at the accompanying website (http://booksupport.wiley.com).

Many of the ideas and changes that formed the basis for this third edition came from numerous discussions with colleagues. I would like to thank Henk De Feyter, Chathura Kumaragamage, Terry Nixon, Graeme Mason, Kevin Behar, and Douglas Rothman for many fruitful discussions.

Finally, I would like to acknowledge the contributions of original data from Dan Green and Simon Pittard (Magnex Scientific), Wolfgang Dreher (University of Bremen), Andrew Maudsley

(University of Miami), Yanping Luo and Michael Garwood (University of Minnesota), Bart Steensma, Dennis Klomp, Kees Braun, Jan van Emous, and Cees van Echteld (Utrecht University), and Henk De Feyter, Zachary Corbin, Robert Fulbright, Graeme Mason, Terry Nixon, Laura Sacolick, and Gerald Shulman (Yale University).

May 2018

Robin A. de Graaf
New Haven, CT, USA

Abbreviations

1D	one-dimensional
2D	two-dimensional
2HG	2-hydoxyglutarate
3D	three-dimensional
5-FU	5-fluoruracil
AC	alternating current
Ace	acetate
ADC	analog-to-digital converter
ADC	apparent diffusion coefficient
ADP	adenosine diphosphate
AFP	adiabatic full passage
AHP	adiabatic half passage
Ala	alanine
Asc	ascorbic acid
Asp	aspartate
ATP	adenosine triphosphate
BHB	β-hydroxy-butyrate
BIR	B_1-insensitive rotation
BISEP	B_1-insensitive spectral editing pulse
BOLD	blood oxygen level-dependent
BPP	Bloembergen, Purcell, Pound
BS	Bloch–Siegert
CBF	cerebral blood flow
CBV	cerebral blood volume
CEST	chemical exchange saturation transfer
CHESS	chemical shift selective
Cho	choline-containing compounds
CK	creatine kinase
CMR_{Glc}	cerebral metabolic rate of glucose consumption
CMR_{O_2}	cerebral metabolic rate of oxygen consumption
COSY	correlation spectroscopy
CPMG	Carr–Purcell–Meiboom–Gill
Cr	creatine
CRLB	Cramer–Rao lower bound
Crn	carnitine
CSDA	chemical shift displacement artifact
CSDE	chemical shift displacement error

CSF	cerebrospinal fluid
CW	continuous wave
DANTE	delays alternating with nutation for tailored excitation
dB	decibel
DC	direct current
DEFT	driven equilibrium Fourier transform
DEPT	distortionless enhancement by polarization transfer
DMb	deoxymyoblobin
DMI	deuterium metabolic imaging
DNA	deoxyribonucleic acid
DNP	dynamic nuclear polarization
DQC	double quantum coherence
DSS	2,2-dimethyl-2-silapentane-5-sulfonate
DSV	diameter spherical volume
DTI	diffusion tensor imaging
EA	ethanolamine
EMCL	extramyocellular lipids
EMF	electromotive force
EPI	echo planar imaging
EPSI	echo planar spectroscopic imaging
FDG	2-fluoro-2-deoxy-glucose
FDG-6P	2-fluoro-2-deoxy-glucose-6-phosphate
FFT	fast Fourier transformation
FID	free induction decay
FLASH	fast low-angle shot
fMRI	functional magnetic resonance imaging
FOCI	frequency offset corrected inversion
FOV	field of view
FSW	Fourier series windows
FT	Fourier transformation
FWHM	Frequency width at half maximum
GABA	γ-aminobutyric acid
GE	gradient echo
Glc	glucose
Gln	glutamine
Glu	glutamate
Glx	glutamine and glutamate
Gly	glycine
GOIA	gradient-offset-independent adiabaticity
GPC	glycerophosphorylcholine
GPE	glycerophosphorylethanolamine
GRAPPA	generalized autocalibrating partially parallel acquisitions
GSH	glutathione (reduced form)
HLSVD	Hankel Lanczos singular value decomposition
HMPT	hexamethylphosphorustriamide
HMQC	heteronuclear multiple quantum correlation
HSQC	heteronuclear single quantum correlation
Ile	isoleucine

IMCL	intramyocellular lipids
INEPT	insensitive nuclei enhanced by polarization transfer
IR	inversion recovery
ISIS	image-selected *in vivo* spectroscopy
IT	inversion transfer
IVS	inner volume selection
JR	jump-return
JRES	J-resolved spectroscopy
Lac	lactate
LASER	localization by adiabatic selective refocusing
Leu	leucine
Mb	myoglobin
MC	multi-coil
MEGA	Mescher–Garwood
mI	*myo*-inositol
MLEV	Malcolm Levitt
MM	macromolecules
MQC	multiple quantum coherence
MRF	magnetic resonance fingerprinting
MRI	magnetic resonance imaging
MRS	magnetic resonance spectroscopy
MRSI	magnetic resonance spectroscopic imaging
MT	magnetization transfer
MTC	magnetization transfer contrast
NAA	*N*-acetyl aspartate
NAAG	*N*-acetyl aspartyl glutamate
NAD(H)	nicotinamide adenine dinucleotide oxidized (reduced)
NADP(H)	nicotinamide adenine dinucleotide phosphate oxidized (reduced)
NDP	nucleoside diphosphate
NMR	nuclear magnetic resonance
nOe	nuclear Overhauser effect (or enhancement)
NOESY	nuclear Overhauser effect spectroscopy
NTP	nucleoside triphosphate
OSIRIS	outer volume suppressed image-related *in vivo* spectroscopy
OVS	outer volume suppression
PCA	perchloric acid
PCr	phosphocreatine
PDE	phosphodiesters
PE	phosphorylethanolamine
PET	positron emission tomography
PFC	perfluorocarbons
PHIP	para-hydrogen-induced polarization
P_i	inorganic phosphate
PME	phosphomonoesters
POCE	proton-observed carbon-edited
PPM	parts per million
PRESS	point resolved spectroscopy
PSF	point spread function

QSM	quantitative susceptibility mapping
QUALITY	quantification by converting line shapes to the Lorentzian type
RAHP	time-reversed adiabatic half passage
RARE	rapid acquisition, relaxation enhanced
RF	radiofrequency
RMS	root mean squared
RNA	ribonucleic acid
ROI	region of interest
SABRE	signal amplification by reversible exchange
SAR	specific absorption rate
SE	spin-echo
SENSE	sensitivity encoding
SEOP	spin-exchange optical pumping
SH	spherical harmonics
sI	*scyllo*-inositol
SI	spectroscopic imaging
SLIM	spectral localization by imaging
SLR	Shinnar–Le Roux
S/*N*	signal-to-noise ratio
SNR	signal-to-noise ratio
SPECIAL	spin-echo, full intensity acquired localized
SQC	single quantum coherence
SSAP	solvent suppression adiabatic pulse
SSFP	steady-state free precession
ST	saturation transfer
STE	stimulated echo
STEAM	stimulated echo acquisition mode
SV	single voxel (or volume)
SVD	singular value decomposition
SWAMP	selective water suppression with adiabatic-modulated pulses
Tau	taurine
TCA	tricarboxylic acid
tCho	total choline
tCr	total creatine
TEM	transverse electromagnetic mode
Thr	threonine
TMA	trimethylammonium
TMS	tetramethylsilane
TOCSY	total correlation spectroscopy
TPPI	time proportional phase incrementation
Trp	tryptophan
TSP	3-(trimethylsilyl)-propionate
Tyr	tyrosine
UV	ultraviolet
Val	valine
VAPOR	variable pulse powers and optimized relaxation delays
VARPRO	variable projection
VERSE	variable rate selective excitation

VNA	variable nutation angle
VOI	volume of interest
VSE	volume selective excitation
WALTZ	wideband alternating phase low-power technique for zero residue splitting
WEFT	water eliminated Fourier transform
WET	water suppression enhanced through T_1 effects
ZQC	zero quantum coherence

Symbols

A	absorption frequency domain signal
A_n, B_n	Fourier coefficients
b	b-value (in s/m^2)
b	b-value matrix
B_0	external magnetic field (in T)
B_1	magnetic radiofrequency field of the transmitter (in T)
$B_{1\max}$	maximum amplitude of the irradiating B_1 field (in T)
$B_{1\mathrm{rms}}$	root mean square B_1 amplitude of a RF pulse (in T)
B_{1x}, B_{1y}	real and imaginary components of the irradiating B_1 field (in T)
B_2	magnetic, radiofrequency field of the decoupler (in T)
B_e	effective magnetic field in the laboratory and frequency frames (in T)
$B_\mathrm{e}^{'}$	effective magnetic field in the second rotating frame (in T)
B_loc	local magnetic field (in T)
C	capacitance (in F)
C	correction factor for calculating absolute concentrations
D	(apparent) diffusion coefficient (in m^2 s^{-1})
D	(apparent) diffusion tensor
D	dispersion frequency domain signal
E	energy (in J)
F	Nyquist frequency (in 1 s^{-1})
F	noise figure (in dB)
$f_B(t)$	normalized RF amplitude modulation function
$f_\nu(t)$	normalized RF frequency modulation function
G	magnetic field gradient strength (in T m^{-1})
$G(t)$	correlation function
h	Planck's constant ($6.626\,208 \times 10^{-34}$ Js)
$\boldsymbol{H}$	Hadamard matrix
I	imaginary time- or frequency-domain signal
I	spin quantum number
I_0	Boltzmann equilibrium magnetization for spin I
I_{nm}	shim current for shim coil of order n and degree m
J	spin–spin or scalar coupling constant (in Hz)
J_0	zero-order Bessel function
$J(\nu)$	spectral density function
k	Boltzmann equilibrium constant ($1.380\,66 \times 10^{-23}$ J K^{-1})
k	k-space variable (in m^{-1})
k_f	k-space variable in frequency-encoding direction (in m^{-1})
k_p	k-space variable in phase-encoding direction (in m^{-1})

k_{AB}, k_{BA}	unidirectional rate constants (in s^{-1})
k_{for}	forward, unidirectional rate constant (in s^{-1})
k_{rev}	reversed, unidirectional rate constant (in s^{-1})
L	inductance (in H)
m	magnetic quantum number
m	mass (in kg)
M	macroscopic magnetization
M	magnitude-mode frequency domain signal
M	mutual inductance (in H)
M_0	macroscopic equilibrium magnetization
M_x, M_y, M_z	orthogonal components of the macroscopic magnetization
N	noise
N	number of phase-encoding increments
N	total number of nuclei or spins in a macroscopic sample
p	order of coherence
Q	quality factor
r	distance (in m)
R	composite pulse (sequence)
R	product of bandwidth and pulse length
R	real time- or frequency-domain signal
R	resistance (in Ω)
R	rotation matrix
R_{1A}, R_{1B}	longitudinal relaxation rate constants for spins A and B in the absence of chemical exchange or cross-relaxation (in s^{-1})
R_2	transverse relaxation rate (in s^{-1})
R_A, R_B	longitudinal relaxation rate constants for spins A and B in the presence of chemical exchange (in s^{-1})
R_H	hydrodynamic radius (in m)
S	measured NMR signal
$S(k)$	spatial frequency sampling function
t	time (in s)
t_1	incremented time in 2D NMR experiments (in s)
t_{1max}	maximum t_1 period in constant time 2D NMR experiments (in s)
t_2	detection period in 2D NMR experiments (in s)
t_{diff}	diffusion time (in s)
t_{null}	time of zero-crossing (nulling) during an inversion recovery experiment (in s)
T	absolute temperature (in K)
T	pulse length (in s)
T_1	longitudinal relaxation time constant (in s)
$T_{1,obs}$	observed, longitudinal relaxation time constant (in s)
T_2	transverse relaxation time constant (in s)
T_2^*	apparent transverse relaxation time constant (in s)
$T_{2,obs}$	observed, transverse relaxation time constant (in s)
T_{acq}	acquisition time (in s)
TE	echo time (in s)
TE_{CPMG}	echo time in a CPMG experiment (in s)
TI	inversion time (in s)
TI1	first inversion time (in s)
TI2	second inversion time (in s)

TM	delay time between the second and third 90° pulses in STEAM (in s)
TR	repetition time (in s)
v	velocity (in $\mathrm{m\,s^{-1}}$)
W	transition probability (in $1\,\mathrm{s^{-1}}$)
W_{nm}	angular function of spherical polar coordinates
$W(k)$	spatial frequency weighting function
x	molar fraction
X_C	capacitive reactance (in Ω)
X_L	inductive reactance (in Ω)
Z	impedance (in Ω)
α	nutation angle (in rad)
β	precession angle of magnetization perpendicular to the effective magnetic field B_e (in rad)
γ	gyromagnetic ratio (in $\mathrm{rad\,T^{-1}\,s^{-1}}$)
δ	chemical shift (in ppm)
δ	gradient duration (in s)
Δ	separation between a pair of gradients (in s)
ΔB_0	magnetic field shift (in T)
$\Delta\nu$	frequency offset (in Hz)
$\Delta\nu_{1/2}$	full width at half maximum of an absorption line (in Hz)
$\Delta\nu_{max}$	maximum frequency modulation of an adiabatic RF pulse (in Hz)
ε	gradient rise time for a trapezoidal magnetic field gradient (in s)
η	nuclear Overhauser enhancement
η	viscosity (in $\mathrm{Ns\,m^{-2}}$)
θ	nutation angle (in rad)
μ	magnetic moment (in $\mathrm{A{\cdot}m^2}$)
μ_0	permeability constant in vacuum ($4\pi{\cdot}10^{-7}\ \mathrm{kg{\cdot}m{\cdot}s^{-2}{\cdot}A^{-2}}$)
μ_e	electronic magnetic moment (in $\mathrm{A{\cdot}m^2}$)
ν_0	Larmor frequency (in Hz)
ν_A	frequency of a non-protonated compound A (in Hz)
ν_{HA}	frequency of a protonated compound HA (in Hz)
ν_{ref}	reference frequency (in Hz)
ξ	electromotive force (in V)
σ	density matrix
τ_c	rotation correlation time (in s)
τ_m	mixing time in 2D NMR experiments (in s)
ϕ	phase (in rad)
ϕ_0	zero-order (constant) phase (in rad)
ϕ_1	first-order (linear) phase (in rad)
ϕ_c	phase correction (in rad)
χ	magnetic susceptibility
ω_0	Larmor frequency (in $\mathrm{rad\,s^{-1}}$)
[]	concentration (in M)

Supplementary Material

To access supplementary materials for this book please use the download links shown below. There you will find valuable material designed to enhance your learning, including:

- Solutions to the exercises in the book
- Download option for PulseWizard
- Short video
- PPTs of all the figures

This book is accompanied by a companion website:

http://booksupport.wiley.com

Please enter the book title, author name or ISBN to access this material.

1

Basic Principles

1.1 Introduction

Spectroscopy is the study of the interaction between matter and electromagnetic radiation. Atoms and molecules have a range of discrete energy levels corresponding to different, quantized electronic, vibrational, or rotational states. The interaction between atoms and electromagnetic radiation is characterized by the absorption and emission of photons with an energy that exactly matches the energy level difference between two states. Since the energy of a photon is proportional to the frequency, the different forms of spectroscopy are often distinguished on the basis of the frequencies involved. For instance, absorption and emission between the electronic states of the outer electrons typically require frequencies in the ultraviolet (UV) range, hence giving rise to UV spectroscopy. Molecular vibrational modes are characterized by frequencies just below visible red light and are thus studied with infrared (IR) spectroscopy. Nuclear magnetic resonance (NMR) spectroscopy uses radiofrequencies, which are typically in the range of 10–1000 MHz.

NMR is the study of the magnetic properties and related energies of nuclei. The absorption of radiofrequency energy can be observed when the nuclei are placed in a (strong) external magnetic field. Purcell et al. [1] at MIT, Cambridge and Bloch et al. [2–4] at Stanford simultaneously, but independently discovered NMR in 1945. In 1952, Bloch and Purcell shared the Nobel Prize in Physics in recognition of their pioneering achievements [5, 6]. At this stage, NMR was purely an experiment for physicists to determine the nuclear magnetic moments of nuclei. NMR could only develop into one of the most versatile forms of spectroscopy after the discovery that nuclei within the same molecule absorb energy at different resonance frequencies. These so-called chemical shift effects, which are directly related to the chemical environment of the nuclei, were first observed in 1949 by Proctor and Yu [7], and independently by Dickinson [8]. The ability of NMR to provide detailed chemical information on compounds was firmly established when Arnold et al. [9] in 1951 published a high-resolution ^{1}H NMR spectrum of ethanol in which separate signals from methyl, methylene, and hydroxyl protons could be clearly recognized.

In the first two decades, NMR spectra were recorded in a continuous wave mode in which the magnetic field strength or the radio frequency was swept through the spectral area of interest, while keeping the other fixed. In 1966, NMR was revolutionized by Ernst and Anderson [10] who introduced pulsed NMR in combination with Fourier transformation. Pulsed or Fourier transform NMR is at the heart of all modern NMR experiments.

The induced energy level difference of nuclei in an external magnetic field is very small when compared to the thermal energy at room temperature, making it that the energy levels

In Vivo *NMR Spectroscopy: Principles and Techniques*, Third Edition. Robin A. de Graaf.

are almost equally populated. As a result the absorption of photons is very low, making NMR a very insensitive technique when compared to the other forms of spectroscopy. However, the low-energy absorption makes NMR also a noninvasive and nondestructive technique, ideally suited for *in vivo* measurements. It is believed that, by observing the water signal from his own finger, Bloch was the first to perform an *in vivo* NMR experiment. Over the following decades, NMR studies were carried out on various biological samples like vegetables and mammalian tissue preparations. Continued interest in defining and explaining the properties of water in biological tissues led to the promising report of Damadian in 1971 [11] that NMR properties (relaxation times) of malignant tumorous tissues significantly differs from normal tissue, suggesting that proton NMR may have diagnostic value. In the early 1970s, the first experiments of NMR spectroscopy on intact living tissues were reported. Moon and Richards [12] used ^{31}P NMR on intact red blood cells and showed how the intracellular pH can be determined from chemical shift differences. In 1974, Hoult et al. [13] reported the first study of ^{31}P NMR to study intact, excised rat hind leg. Acquisition of the first ^{1}H NMR spectra was delayed by almost a decade due to technical difficulties related to spatial localization, and water and lipid suppression. Behar et al. [14] and Bottomley et al. [15] reported the first ^{1}H NMR spectra from rat and human brain, respectively. Since the humble beginnings, *in vivo* MR spectroscopy (MRS) has grown as an important technique to study static and dynamic aspects of metabolism in disease and in health.

In parallel with the onset of *in vivo* MRS, the world of high-resolution, liquid-state NMR was revolutionized by the introduction of 2D NMR by Ernst and coworkers [16] based on the concept proposed by Jeener in 1971 [17]. The development of hundreds of 2D methods in the following decades firmly established NMR as a leading analytical tool in the identification and structure determination of low-molecular weight chemicals. Richard Ernst was awarded the 1991 Nobel Prize in Chemistry for his contributions to the methodological development of NMR [18]. The application of multidimensional NMR to the study of biological macromolecules allowed determination of the 3D structure of proteins in an aqueous environment, providing an alternative to X-ray crystallography. Kurt Wuthrich was awarded the 2002 Nobel Prize in Chemistry for his contributions to the development of protein NMR and 3D protein structure determination [19].

Around the same time reports on *in vivo* MRS appeared, Lauterbur [20] and Mansfield and Grannell [21] described the first reports on a major constituent of modern NMR, namely *in vivo* NMR imaging or magnetic resonance imaging (MRI). By applying position-dependent magnetic fields in addition to the static magnetic field, they were able to reconstruct the spatial distribution of nuclear spins in the form of an image. Lauterbur and Mansfield shared the 2003 Nobel Prize in Medicine [22, 23]. Since its inception, MRI has flourished to become the leading method for structural and functional imaging with methods like diffusion tensor imaging (DTI) and blood oxygenation level-dependent (BOLD) functional MRI.

As a leading clinical and research imaging modality, the theoretical and practical aspects of MRI are covered in a wide range of excellent textbooks [24–26]. While MRS is based on the same fundamental principles as MRI, the practical considerations for high-quality MRS are very different. This book is dedicated to providing a robust description of current *in vivo* MRS methods, with an emphasis on practical challenges and considerations. This chapter covers the principles of NMR that are common to both MRI and MRS. Starting with classical arguments, the concepts of precession, coherence, resonance, excitation, induction, and relaxation are explained. The quantum mechanical view of NMR is briefly reviewed after which the phenomena of chemical shift and scalar coupling will be described, as well as some elementary processing of the NMR signal.

1.2 Classical Magnetic Moments

The discovery of NMR by Bloch and Purcell in 1945 was not a serendipitous event, but was based on the work by Rabi [27, 28] in the previous decade on magnetic resonance of individual particles in a molecular beam for which he received the 1944 Nobel Prize in Physics. While both groups reported the detection of signal associated with proton magnetic moments, the experimental setups as well as the conceptualization of the NMR phenomenon were very different.

Bloch approached NMR from a classical point of view in which the orientation of magnetic moments is gradually changed by an oscillating magnetic field. This would ultimately lead to the detection of NMR signal from water protons through electromagnetic induction in a nearby receiver coil. Purcell viewed the NMR phenomenon based on quantum mechanics, in close analogy to other spectroscopic methods in which transitions are induced between energy levels by quanta of energy provided by radiofrequency (RF) waves. Purcell described the absorption of energy provided by an oscillating RF field by the protons in solid paraffin. A wonderful overview of the two discoveries of NMR is given by Rigden [29] and Becker et al. [30] as well as by the Nobel lectures of Bloch [5] and Purcell [6].

The spectroscopic or quantum mechanical view often takes center stage in the introduction of many text books, including the previous editions of this book. The main reason for this approach is that a full quantum mechanical description of NMR can account for all observed phenomena, including those that have no classical analog, like scalar or J-coupling. However, as the quantum description of NMR does not deal directly with observable magnetization, but rather with the energetic state of the system, it does not provide an intuitive, physical picture. In the classical view of NMR, the magnetic moments of the individual nuclear spins are summed up to form a macroscopic magnetization vector that can be followed over time using classical electromagnetism concepts. This provides a familiar picture that can be used to follow the fate of magnetization under a wide range of experimental conditions. The classical picture is advocated here, starting with a magnetized needle as found in a compass.

As with all magnets, the compass needle is characterized by a magnetic north and south pole from which the magnetic field lines exit and enter the needle, respectively (Figure 1.1A). The magnetic field lines shown in Figure 1.1A can be summarized by a magnetic moment, μ, describing both the amplitude and direction. In the absence of an external magnetic field the compass needle has no preference in spatial orientation and can therefore point in any direction.

When placed in an external magnetic field, such as the Earth's magnetic field, the compass needle experiences a torque (or rotational force) that rotates the magnetic moment towards a parallel orientation with the external field (Figure 1.1B). As the magnetic moment "overshoots" the parallel orientation, the torque is reversed and the needle will settle into an oscillation or frequency that depends on the strengths of the external magnetic field and the magnetic moment. Due to friction between the needle and the mounting point, the amplitude of the oscillation is dampened and will ultimately result in the stabile, parallel orientation of the needle with respect to the external field (Figure 1.1C) representing the lowest magnetic energy state (the antiparallel orientation represents the highest magnetic energy state).

The equilibrium situation (Figure 1.1C) can, besides mechanical means, be perturbed by additional magnetic fields as shown in Figure 1.1D. When a bar magnet is moved towards the compass, the needle experiences a torque and is pushed away from the parallel orientation. When the bar magnet is removed, the needle oscillates as shown in Figure 1.1B before returning to the equilibrium situation (Figure 1.1C). However, if the bar magnet is moved back and

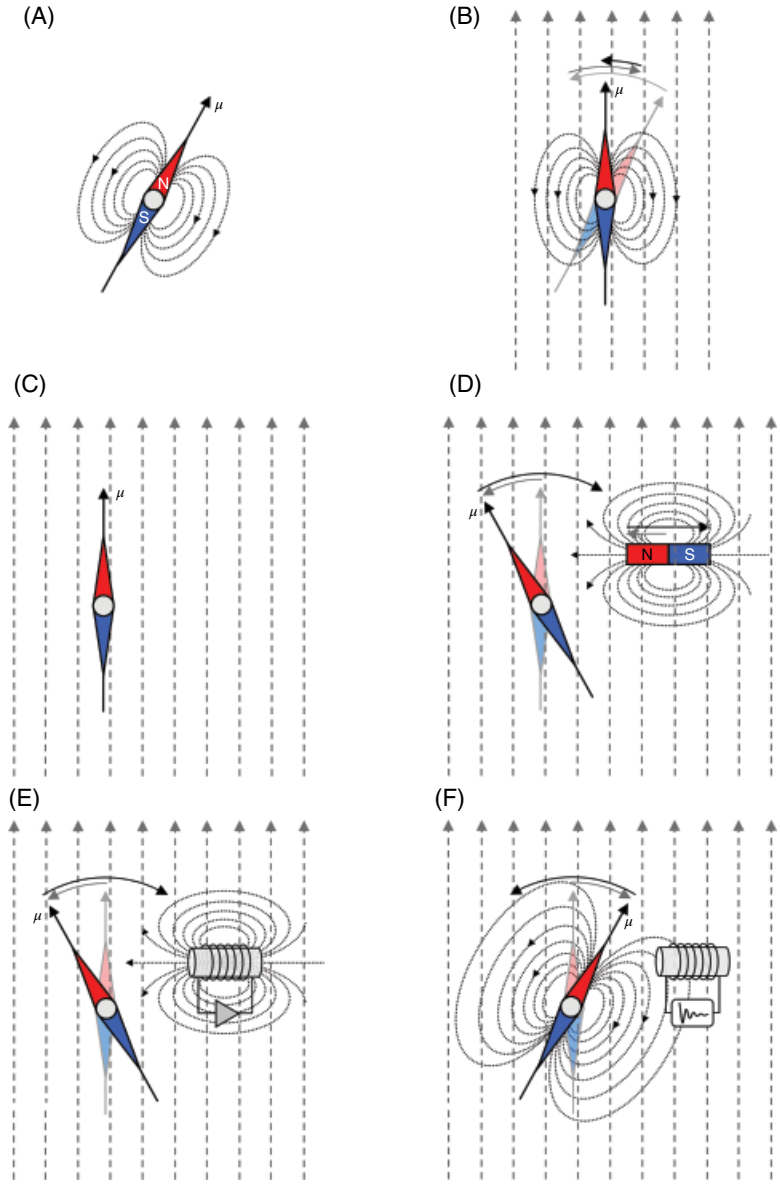

Figure 1.1 Oscillations of a classical compass needle. (A) A compass needle with a magnetic north and south pole creates a dipolar magnetic field distribution of which the amplitude and direction are characterized by the magnetic moment μ. (B) When placed in an external magnetic field the magnetic moment oscillates a number of times before (C) settling in a parallel orientation with the external magnetic field. Note that in Earth's magnetic field the compass needle points to the magnetic south, which happens to be close to geographical north. (D) The needle can be perturbed with a bar magnet, whereby the perturbation reaches maximum effect when the bar movement matches the natural frequency of the needle. (E) The bar magnet can be replaced by an alternating current in a coil. (F) The same coil can also be used to detect the oscillating magnetic moment of the needle through electromagnetic induction.

forth relative to the compass, the needle can be made to oscillate continuously. When the movement frequency of the bar magnet is very different from the natural frequency of the needle (Figure 1.1B), the effect of the bar magnet is not constructive and the needle never deviates far from the parallel orientation. However, when the frequency of the bar magnet

movement matches the natural frequency of the needle, the repeated push from the bar magnet on the needle is constructive and the needle will deviate increasingly further from the parallel orientation. When the bar magnet has a maximum effect on the needle, the system is in resonance and the oscillation is referred to as the resonance frequency. A similar situation arises when pushing a child in a swing; only when the child is pushed in synchrony with the natural or resonance frequency of the swing set does the amplitude get larger.

The bar magnet can be replaced with an alternating current in a copper coil as shown in Figure 1.1E. The alternating current generates a time-varying magnetic field that can perturb the compass needle. When the frequency of the alternating current matches the natural frequency of the needle, the system is in resonance and large deviations of the needle can be observed with modest, but constructive "pushes" from the magnetic field produced by the coil.

The compass needle continues to oscillate at the natural frequency for some time following the termination of the alternating current (Figure 1.1F). The compass needle creates a time-varying magnetic field that can be detected through Faraday electromagnetic induction in the same coil previously used to perturb the needle. The induced voltage, referred to as the Free Induction Decay (FID), will oscillate at the natural frequency and will gradually reduce in amplitude as the compass needle settles into the parallel orientation.

Figure 1.1 shows that the MR part of NMR can be completely described by classical means. It is therefore also not surprising that Bloch titled his seminal paper "Nuclear induction" [2, 4] as the electromagnetic induction is an essential part of MR detection. The magnetic effects summarized in Figure 1.1 are readily reproduced "on the bench" and provide an excellent means of experimentally demonstrating some of the concepts of MR [31].

1.3 Nuclear Magnetization

Any rotating object is characterized by angular momentum, describing the tendency of the object to continue spinning. Subatomic particles like electrons, neutrons, and protons have an *intrinsic* angular moment, or spin that is there even though the particle is not actually spinning. Electron spin results from relativistic quantum mechanics as described by Dirac in 1928 [32] and has no classical analog. For the purpose of this book the existence of spin is simply taken as a feature of nature. Particles with spin always have an intrinsic magnetic moment. This can be conceptualized as a magnetic field generated by rotating currents within the spinning particle. This should, however, not be taken too literal as the particle is not actually rotating. Note that in the NMR literature, spin and magnetic moments are used interchangeably.

Protons are abundantly present in most tissues in the form of water or lipids. In the human brain, a small cubic volume of $1 \times 1 \times 1$ mm contains about 6×10^{19} proton spins (Figure 1.2A and B). In the absence of an external magnetic field, the spin orientation has no preference and the spins are randomly oriented throughout the sample (Figure 1.2B). For a large number of spins this can also be visualized by a "spin-orientation sphere" (Figure 1.2C) in which each spin has been placed in the center of a Cartesian grid. Summation over all orientations leads to a (near) perfect cancelation of the magnetic moments and hence to the absence of a macroscopic magnetization vector. It should be noted that the concept of a spin-orientation sphere has been used throughout the NMR literature [33–35], albeit sporadically. The description of the NMR phenomenon based on a spin-orientation sphere will be advocated here as a classical, intuitive alternative to the quantum-mechanical view.

Up to this point the nuclear magnetic moments behave similarly to the magnetic moments associated with classical compass needles. However, unlike compass needles nuclear magnetic moments have intrinsic angular momentum or spin which can be visualized as a nucleus spinning around its own axis (Figure 1.2D). When a nuclear spin is placed in an external

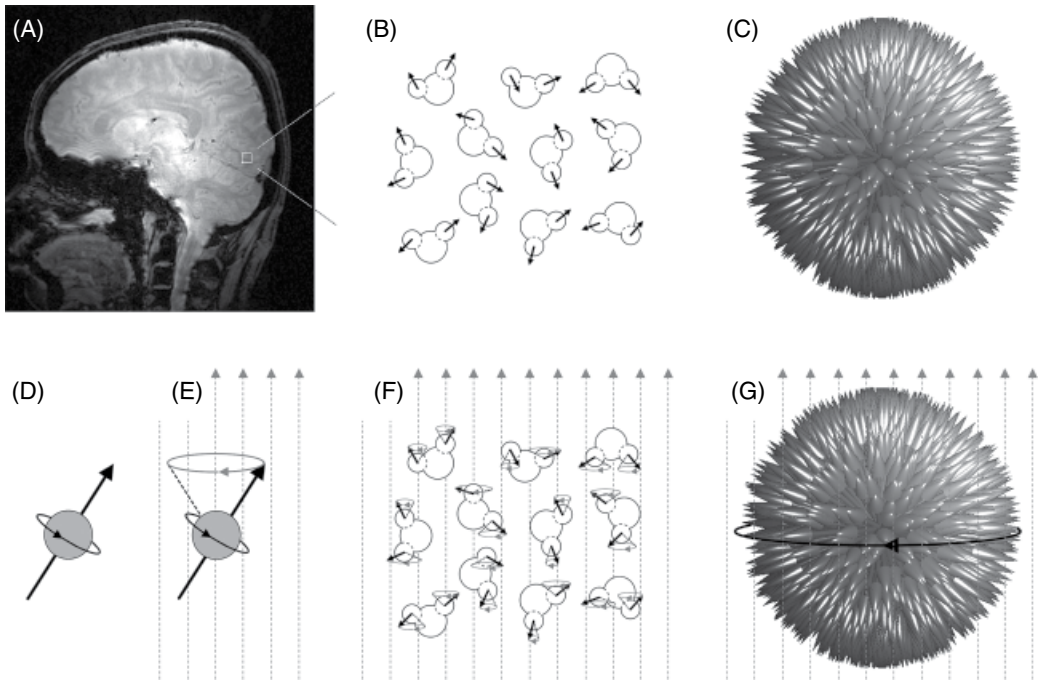

Figure 1.2 Precession of nuclear spins. (A, B) A small 1 µl volume from the human brain contains about 6×10^{19} protons, primarily located in water molecules. (B, C) In the absence of a magnetic field the proton spins have no orientational preference, leading to a randomly distributed "spin-orientation sphere." (D) Unlike compass needles, nuclear magnetic moments have intrinsic angular momentum or spin that leads to (E) a precessional motion when placed in a magnetic field. (F) All spins attain Larmor precession, but retain their random orientation to a good first approximation. (G) While the spin-orientation sphere also remains random when placed in a magnetic field, the entire sphere will attain Larmor precession.

magnetic field (Figure 1.2E) the presence of angular momentum makes the magnetic moment precess around the external magnetic field (Figure 1.2E). This effect is referred to as Larmor precession and the corresponding Larmor frequency ν_0 (in MHz) is given by

$$\nu_0 = \frac{\omega_0}{2\pi} = \frac{\gamma}{2\pi} B_0 \tag{1.1}$$

where γ is the gyromagnetic (or magnetogyric) ratio (in rad·MHz T^{-1}) and B_0 is the magnetic field strength (in T). The gyromagnetic ratio, which is constant for a given nucleus, is tabulated in Table 1.1. For protons at 7.0 T the Larmor frequency is 298 MHz. It should be noted that Larmor precession occurs for any spinning magnetic moment in a magnetic field, including classical objects and that it was described decades before the discovery of NMR [36].

When the protons depicted in Figure 1.2B are subjected to an external magnetic field, every spin starts to precess around the magnetic field with the same Larmor frequency. The Larmor frequency is independent of the angle between the external magnetic field and an individual spin. As the orientation of the magnetic moment with respect to the main magnetic field does (initially) not change, the spin-orientation sphere representation of Figure 1.2C remains unchanged with the exception that the entire sphere is rotating around the magnetic field at the Larmor frequency. If Larmor precession would be the only effect induced by the external magnetic field, then NMR would never have developed into the versatile technique as we know it today.

Table 1.1 NMR properties of biologically relevant nuclei encountered in *in vivo* NMR.

Isotope	Spin	Gyromagnetic ratio (rad·MHzT^{-1})	NMR frequency ratio (% of ^{1}H)	Natural abundance (%)
^{1}H	1/2	267.522	100.000	99.985
^{2}H	1	41.066	15.351	0.015
^{3}He	1/2	−203.802	76.179	0.000 14
^{7}Li	3/2	103.977	38.864	92.58
^{13}C	1/2	67.283	25.145	1.108
^{14}N	1	19.338	7.226	99.630
^{15}N	1/2	−27.126	10.137	0.370
^{17}O	5/2	−36.281	13.556	0.037
^{19}F	1/2	251.815	94.094	100.000
^{23}Na	3/2	70.808	26.452	100.000
^{29}Si	1/2	−53.190	19.867	4.7
^{31}P	1/2	108.394	40.481	100.000
^{33}S	3/2	20.557	7.676	0.76
^{35}CI	3/2	26.242	9.798	75.53
^{37}CI	3/2	21.844	8.156	24.47
^{39}K	3/2	12.501	4.667	93.100
^{129}Xe	1/2	−74.521	27.810	26.44

Fortunately, there is a second, more subtle effect that ultimately leads to a net, macroscopic magnetization vector that can be detected. The water molecules in Figure 1.2B are in the liquid state and therefore undergo molecular tumbling with a range of rotations, translations, and collisions. As a result, the amplitude and orientation of the magnetic field generated by one proton at the position of another proton changes over time (Figure 1.3A). When the local field fluctuation matches the Larmor frequency, it can perturb the spin orientation. These perturbations are largely, but not completely, random. The presence of a strong external magnetic field slightly favors the parallel spin orientation. As a result, over time the completely random spin orientation distribution (Figure 1.3B) changes into a distribution that is slightly biased towards a parallel spin orientation (Figure 1.3C). Visually, the spin distributions in the absence (Figure 1.3B) and presence (Figure 1.3C) of an external magnetic field look similar because the net number of spins that are biased towards the parallel orientation is very small, on the order of one in a million. The situation becomes visually clearer when the spin distribution is separated into spins that have a random orientation distribution (Figure 1.3D) and spins that are slightly biased towards a parallel orientation (Figure 1.3E). Adding the magnetic moments of Figure 1.3D does not lead to macroscopic magnetization similar to the situation in Figure 1.2G. However, adding the magnetic moments of Figure 1.3E leads to a macroscopic magnetization vector parallel to the external magnetic field. As the external magnetic field only biases the spin distribution along its direction, the spin distribution in the two orthogonal, transverse directions is still random.

The microscopic processes detailed in Figure 1.3A–E can be summarized at a macroscopic level as shown in Figure 1.3F. In the absence of a magnetic field ($t < 0$) the sample does not produce macroscopic magnetization. When an external magnetic field is instantaneously turned on ($t = 0$), the macroscopic magnetization exponentially grows over time where it plateaus at

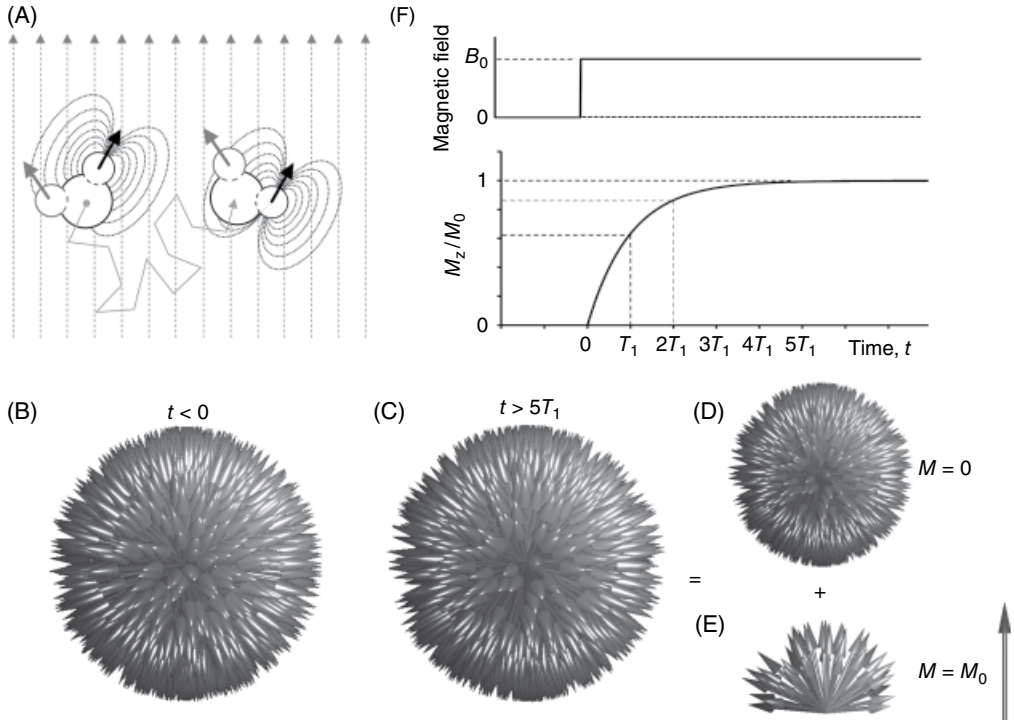

Figure 1.3 Appearance of macroscopic magnetization through T_1 relaxation. (A) Molecular tumbling and Brownian motion causes spin 1 (gray) to experience a wide range of magnetic field fluctuations originating from spin 2 (black) and other spins outside the water molecule. Magnetic field fluctuations of the proper frequency can change the spin orientation. While the perturbations are largely random, there is a very slight bias towards a parallel orientation with the external magnetic field. Over time the almost random perturbations transform a completely random spin-orientation sphere (B) into one that has a small polarization M_0 (C). The small polarization M_0 can be visualized better when the spins with a random orientation (D) are separated from the spins that have attained a slight bias (E). (F) Macroscopically the small polarization M_0 appears exponentially over time with a characteristic T_1 relaxation time constant according to Eq. (1.2).

a value corresponding to the thermal equilibrium magnetization, M_0. The appearance of macroscopic magnetization can be described by

$$M_z(t) = M_0 - \left(M_0 - M_z(0)\right)e^{-t/T_1} \tag{1.2}$$

where T_1 is the longitudinal relaxation time constant and $M_z(0)$ is the longitudinal magnetization at time zero. In the case of Figure 1.3, the initial longitudinal magnetization is zero, i.e. $M_z(0) = 0$. At the time of the first NMR studies, little was known about T_1 relaxation times in bulk matter. Both originators of NMR, Bloch and Purcell, were acutely aware that a very long T_1 relaxation time constant could seriously complicate the detection of nuclear magnetism. As a precaution, Purcell used an exceedingly small RF field such as not to saturate the sample [1], whereas it is rumored that Bloch left his sample in the magnet to reach thermal equilibrium while on a skiing trip [29]. Following the initial experiments it became clear that T_1 relaxation time constants can range from milliseconds to minutes, with water establishing thermal equilibrium in seconds. Extraordinarily long T_1 relaxation times may, however, have been the main reason for earlier, negative reports by Gorter [37, 38] on the detection of NMR in bulk matter.

The longitudinal magnetization vector represents the signal that will be detected in an NMR experiment. However, the static, longitudinal magnetization is never detected directly as its